Non-innocent behavior of 1-(2′-pyridylazo)-2-naphtholate coordinated to polypyridine ruthenium(II) complexes

Kalil C.F. Toledo[ab], Tiago A. Matias[c], Herculys B. Jorge[a], Henrique E. Toma[c], Juliano A. Bonacin[b] & Vagner R. de Souza[a]

[a] Department of Chemistry, State University of Maringá, Maringá, Brazil

[b] Institute of Chemistry, University of Campinas – UNICAMP, Campinas-SP, Brazil

[c] Institute of Chemistry, University of Sao Paulo, Sao Paulo, Brazil
Accepted author version posted online: 08 Sep 2014.Published online: 26 Sep 2014.

Click for updates

PLEASE SCROLL DOWN FOR ARTICLE

Taylor & Francis
Taylor & Francis Group

# Non-innocent behavior of 1-(2′-pyridylazo)-2-naphtholate coordinated to polypyridine ruthenium(II) complexes

KALIL C.F. TOLEDO†‡, TIAGO A. MATIAS§, HERCULYS B. JORGE†,
HENRIQUE E. TOMA§, JULIANO A. BONACIN‡ and VAGNER R. DE SOUZA*†

†Department of Chemistry, State University of Maringá, Maringá, Brazil
‡Institute of Chemistry, University of Campinas – UNICAMP, Campinas-SP, Brazil
§Institute of Chemistry, University of Sao Paulo, Sao Paulo, Brazil
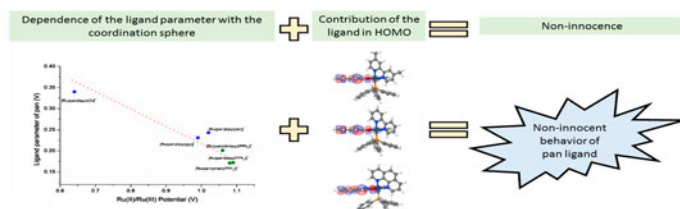
The study of non-innocent redox behavior of ligands is important for the development of new catalysts and to comprehend the function of bioinorganic molecules in biochemical processes. In this work, we present a description of the non-innocent behavior of 1-(2′-pyridylazo)-2-naphtholate (pan) coordinated to ruthenium complexes. The synthesis and characterization of a series of [Ru(pan)(PPh$_3$)(L)]PF$_6$ complexes [where L = 2,2′-bipyridine (bpy), 4,4′-dimethyl-2,2′-bipyridine (dmbpy), and 1,10-phenanthroline (phen)] are presented. UV–vis analyses of the studied ruthenium complexes show intense absorptions from intraligand π–π* and metal-to-ligand charge-transfer transitions bands in the visible region. This observation shows a significant contribution of the pan ligand in all electronic transitions and is the indicative of non-innocent behavior. Theoretical calculations were carried out to support the UV–vis spectral assignments. Non-innocent behavior of pan was observed and confirmed using the electrochemical parameter $E_L(L)$ and by electrochemical studies. The pan ligand is non-innocent and can be modulated by donor and acceptor character of the other ligands present in the coordination sphere of the complex.

Keywords: Ruthenium; Non-innocent ligand; Pan; Electrochemical parameter; Theoretical calculation

1. Introduction

Electronic, catalytic, and spectroscopic properties of coordination compounds can be modulated by metal, oxidation state, and geometry of the complex. In addition, ligands play an important role in the final properties of the complexes. The choice of appropriate ligands

---

*Corresponding author. Email: vrsouza2@uem.br

allows the design of molecular devices with specific characteristics, and this has been the focus of the research of many coordination chemists [1–3].

Based on the interesting properties and wide applications of coordination compounds, it is possible to highlight pyridylazo ligands with multifunctional features [4]. These ligands constitute an important class of analytical reagents employed in spectrophotometric analysis, amperometric determination of metal ions, and as indicators in complexometric titrations [5]. Although coordination of pyridylazo and its derivatives to metals has been extensively investigated [6–10], there are limited number of articles that discuss reactions between pyridylazo ligands and ruthenium complexes [11, 12]. In addition, there is a lack of relevant information concerning spectroscopic and electrochemical properties of these complexes.

Our interest on metal complexes with ligands exhibiting variable degrees of σ-basicity and π-acidity [13–16] led us to investigate the properties of ruthenium complexes with 1-(2′-pyridylazo)-2-naphtholate (pan). This ligand has donor and acceptor behavior, with which it is possible to observe π-acceptor properties in the pyridylazo fragment to stabilize low oxidation states, while naphtholate behaves as a strong σ-donor and stabilizes high oxidation states in transition metal [17].

Relationships between redox properties and the donor ligand properties have been studied by Lever [18], who has assumed the existence of electrochemical additivity relationships [19, 20] allowing assignment of an electrochemical parameter (E_L) for wide range of compounds [21–23]. However, only few classes of ligands have the value of E_L constant. Compounds termed non-innocent ligands [24] exhibit electrochemical parameter changes according to modification of the coordination sphere.

Conceptual definitions about innocent and non-innocent ligands were initially proposed by Jørgensen [25], who assumed that "ligands are innocents when they allow oxidation states of the central atom to be defined." However, the best definition of non-innocent behavior is considering the elevated overlap of the molecular orbitals of the metal and ligand [25–27]. This phenomenon produces a huge electron delocalization in the highest occupied molecular orbital (HOMO) and the oxidation state of the metal is uncertain [28, 29].

Such characteristics allow non-innocent ligands to be commonly found in bioinorganic systems both as substrates (e.g. O_2, NO, and quinones) and as redox active center in porphyrin, dithiolate, and quinone ligands [30]. Due to this non-innocent redox behavior presented by certain ligands coordinated to metals, it is possible to modulate the Lewis acidity of the central metal. These ligands play an important role since they can generate
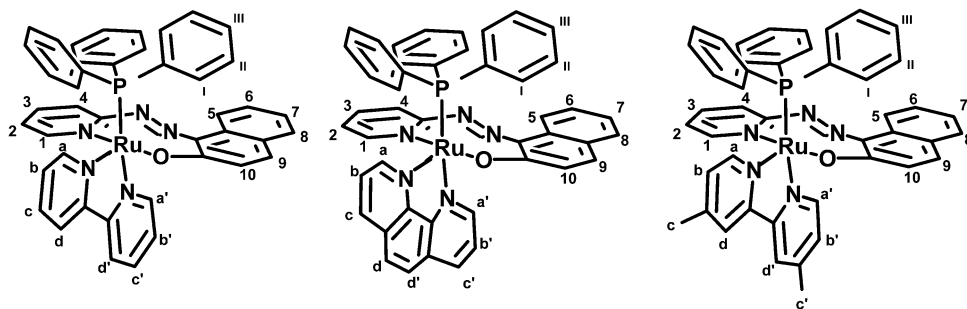

Figure 1. Structural formulas of the ruthenium(II) complexes of 1-(2′-pyridylazo)-2-naphtholate containing bpy, dmbpy, and phen.

reactive ligands–radicals that are capable to break specific chemical bonds in catalytic processes [31].

In this article, a detailed investigation of the non-innocent properties of pan coordinated to ruthenium(II) was carried out. The synthesis, electrochemical behavior, and spectroscopic properties of the complexes, [Ru(pan)(PPh₃)(bpy)]PF₆, [Ru(pan)(PPh₃)(dmbpy)]PF₆, and [Ru(pan)(PPh₃)(phen)]PF₆ (figure 1) are described.

2. Experimental

2.1. *Materials*

1-(2′-Pyridylazo)-2-naphthol (pan), triphenylphosphine, 2,2′-bipyridine (bpy), 4,4′-dimethyl-2,2′-bipyridine (dmbpy), 1,10-phenanthroline (phen), and RuCl₃·3H₂O were purchased from Aldrich Chemical Co. All other solvents and chemicals were reagent grade (Aldrich or Merck) and used without purification. All manipulations were carried out in an inert atmosphere (Ar) following conventional techniques. [Ru(PPh₃)₃Cl₂] and [Ru(pan)(PPh₃)₂Cl] were synthesized by the following reported procedures [12, 32].

2.2. *Synthesis of [Ru(pan)(PPh₃)(bpy)]PF₆*

[Ru(pan)(PPh₃)(bpy)]PF₆ was synthesized by addition of AgNO₃ (0.018 g, 0.10 mM) to a solution of [Ru(pan)(PPh₃)₂Cl] (0.10 g, 0.10 mM) in ethanol (30 cm³). The mixture was heated and stirred for 60 min. Thereafter, the AgCl precipitate was separated by filtration in order to obtain [Ru(pan)(PPh₃)₂(H₂O)]NO₃ in solution. This complex was produced *in situ*, then 2,2′-bipyridine (0.14 g, 0.80 mM) was added. The coordination occurred by the substitution of H₂O ligand by one pyridine from bpy and the second pyridine replaces PPh₃ from the coordination sphere. The resulting solution was heated under reflux for 4 h. It was then concentrated to about 10 cm³ and the desired complex was precipitated by the addition of a saturated aqueous solution of NH₄PF₆ (1.0 cm³). The reddish brown precipitate was collected by filtration, washed with water, and dried in vacuum over P₄O₁₀. The complex was then purified by alumina column chromatography using acetonitrile : dichloromethane (1 : 9) as eluent. Yield 70%. (Found: C, 56.49; H, 3.67; N, 7.12. Calcd for Ru(C₁₅H₁₀N₃O)(PC₁₈H₁₅)(C₁₀H₈N₂)PF₆: C, 56.58; H, 3.62; N, 7.62%). v_{max} (cm⁻¹): 1350s (N=N), 1280s (C–O), 610w (Ru–N), 557w (Ru–O), 524w (Ru–P), 424w (Ru–N).

2.3. *Synthesis of [Ru(pan)(PPh₃)(dmbpy)]PF₆*

[Ru(pan)(PPh₃)(dmbpy)]PF₆ was synthesized by following the same procedure, but using dmbpy (0.15 g) instead of bpy. Yield: 80%. (Found: C, 57.40; H, 3.99; N, 7.42. Calcd for Ru(C₁₅H₁₀N₃O)(PC₁₈H₁₅)(C₁₂H₁₂N₂)PF₆: C, 57.45; H, 3.94; N, 7.45%). v_{max} (cm⁻¹): 1340s (N=N), 1280s (C–O), 605w (Ru–N), 554w (Ru–O), 526w (Ru–P), 420w (Ru–N).

2.4. *Synthesis of [Ru(pan)(PPh₃)(phen)]PF₆*

[Ru(pan)(PPh₃)(phen)]PF₆ was synthesized by following the same procedure described above, but using phen (0.14 g) instead of bpy. Yield: 70%. (Found: C, 57.53; H, 3.59; N,

7.42. Calcd for Ru(C$_{15}$H$_{10}$N$_3$O)(PC$_{18}$H$_{15}$)(C$_{12}$H$_8$N$_2$)PF$_6$: C, 57.69; H, 3.53; N, 7.48%). ν_{max} (cm^{-1}): 1348s (N=N), 1280s (C–O), 610w (Ru–N), 560w (Ru–O), 530w (Ru–P), 428w (Ru–N).

2.5. *Physical measurements*

Elemental analyses were performed in the Perkin–Elmer 2400 CHN Elemental Analyser. Electronic spectra were recorded on a Hewlett–Packard model 8453 A diode array spectrophotometer. IR spectra were obtained in KBr pellets on a Shimadzu FTIR-8300 spectrophotometer. ^{1}H NMR spectra were obtained in a 5 mm NMR tube on a Varian Inova 300 MHz spectrometer in CDCl$_3$ or acetone-d$_6$. Cyclic voltammetry measurements were carried out using a PARC system, from EG&G Instruments, consisting of a potentiostat model 283 and a three electrode cell arrangement. A platinum disk working electrode, a platinum wire auxiliary electrode, Ag/AgNO$_3$ reference electrode ($E°$ = 0.503 V *vs.* NHE) [33], and software ECHEM V. 4.30 were employed for the electrochemical measurements. Solutions of ruthenium complex were prepared in acetonitrile containing 0.10 M cm^{-3} tetraethylammonium perchlorate. All measurements were performed at room temperature, and obtained values were converted to the NHE by the addition of 0.503 V in the electrochemical potential measured. Spectroelectrochemical measurements were carried out using a PARC potentiostat, model 173, in parallel with the Hewlett–Packard diode array spectrophotometer. The quartz spectroelectrochemical cell used has a 0.025 cm optic length and a gold minigrid as working electrode, and platinum wire as auxiliary microelectrode.

2.6. *Theoretical calculation*

All calculations were performed in GAMESS software [34] using the DFT method. The hybrid functional PBE0 was used to solve the Kohn–Sham equation and effective core potential basis set LanL2DZ [35] was employed to ruthenium, while 6-31G(d,p) basis set was used for all others atoms. The geometry optimization was carried out with a convergence criterion of 10^{-3} a.u. in a conjugate gradient algorithm. Theoretical UV–vis spectra including the 20 first states of the complexes were calculated by TD-DFT method (time dependent density functional theory). Total time for each calculation was 300 h and it was performed at the National Center for High Performance (Centro Nacional de Processamento de Alto Desempenho, CENAPAD-UNICAMP).

3. Results and discussion

3.1. *^{1}H NMR*

^{1}H NMR and 2D cozy spectra were used to confirm the proposed structures for ruthenium complexes presented in figure 1. All NMR data were organized according to the type of ligand and assignment, as presented in table 1.

    Aromatic region (δ 6.4–9.4 ppm) is more complex to assign than other regions due to overlap of signals from phosphine and pan protons. The most deshielded doublet is found near 9.4 ppm and is assigned to the proton attached to C1-pan ligand (see figure 1) [12]. ^{1}H

Table 1. ^{1}H NMR chemical shifts (δ, ppm) for the ruthenium(II) complexes.

Ligand	Assignment*	[Ru(pan)(PPh$_3$)(L)]$^{+}$		
		bpy	phen	Dmbpy
pan	H$_1$	9.37	9.39	9.30
	H$_2$	7.53	7.58	7.53
	H$_3$	7.33	7.29	7.20
	H$_4$	6.47	6.42	6.52
	H$_5$	8.58	8.50	8.71
	H$_6$	7.63	7.74	7.16
	H$_7$	7.57	7.65	7.28
	H$_8$	7.49	7.54	7.20
	H$_9$	7.39	7.43	7.40
	H$_{10}$	7.39	7.43	7.40
PPh$_3$	H$_I$	7.19–7.37	7.18–7.32	7.11–7.32
	H$_{II}$	7.19–7.37	7.18–7.32	7.11–7.32
	H$_{III}$	7.19–7.37	7.18–7.32	7.11–7.32
L	H$_a$ (H$_{a'}$)	9.14 (8.87)	9.22 (7.17)	8.36 (8.21)
	H$_b$ (H$_{b'}$)	7.52 (6.92)	7.75 (6.81)	7.12 (6.95)
	H$_c$ (H$_{c'}$)	8.28 (8.17)	8.77 (7.33)	2.67 (2.47)**
	H$_d$ (H$_{d'}$)	8.99 (7.63)	8.75 (8.27)	8.18 (7.05)

*Numbering scheme are shown in figure 1.
**Methyl groups of the ligand dmbpy.

NMR spectra of the complexes show multiple signals for the PPh$_3$ protons at 7.1–7.4 ppm. Spectra of the three complexes show 1 : 1 relation of pan : triphenylphosphine signals, confirming the number of phosphines in the complexes. Absence of the naphtholic proton signal (δ = 16 ppm in free ligand) in complexes suggests coordination by naphtholate – O.

The NMR spectrum of [Ru(pan)(PPh$_3$)(bpy)]$^{+}$, found in figure 2, presents four doublets [H (a) = 9.14 ppm (1H); H(a′) = 8.87 ppm (1H); H(d) = 8.99 ppm (1H); and H(d′) = 7.63 ppm (1H)] and four triplets [H(b) = 7.52 ppm (1H); H(b′) = 6.92 ppm (1H); H(c) = 8.28 ppm (1H); and H(c′) = 8.17 ppm (1H)], which are assigned to protons from aromatic rings of bpy. The spectrum reveals that pyridines of bpy are not equivalent, because C–H (phenyl) of triphenylphosphine is involved in non-covalent interaction with π cloud of bpy and naphthyl ring of pan ligand. Besides hydrogen bonding interactions, intermolecular interactions can be observed such as C–H···π between C–H (pyridyl) from bpy and π-cloud from PPh$_3$.

Spectra of [Ru(pan)(PPh$_3$)(dmbpy)]$^{+}$ and [Ru(pan)(PPh$_3$)(phen)]$^{+}$ are similar to [Ru(pan) (PPh$_3$)(bpy)]$^{+}$, except for methyl group (dmbpy) found at higher magnetic field assigned to 2.67 and 2.47 ppm, and integration calculated as 3 for each.

3.2. *Electronic spectra*

Theoretical calculation was employed to support the understanding about the nature of electronic transitions. All complexes had their geometry optimized by DFT method, as described in Section 2.6. Comparison of theoretical and experimental bond distances between metal and ligand shows a good correlation (see table S1, see online supplemental material at http://dx.doi.org/10.1080/00958972.2014.963064). The errors found in Ru–P bond distance are lower than 1% in all complexes.

The complexes exhibit reddish brown colors in acetonitrile. The spectra of the complexes have intense intraligand π–π* absorptions in the UV region (figure 3). In the visible region,
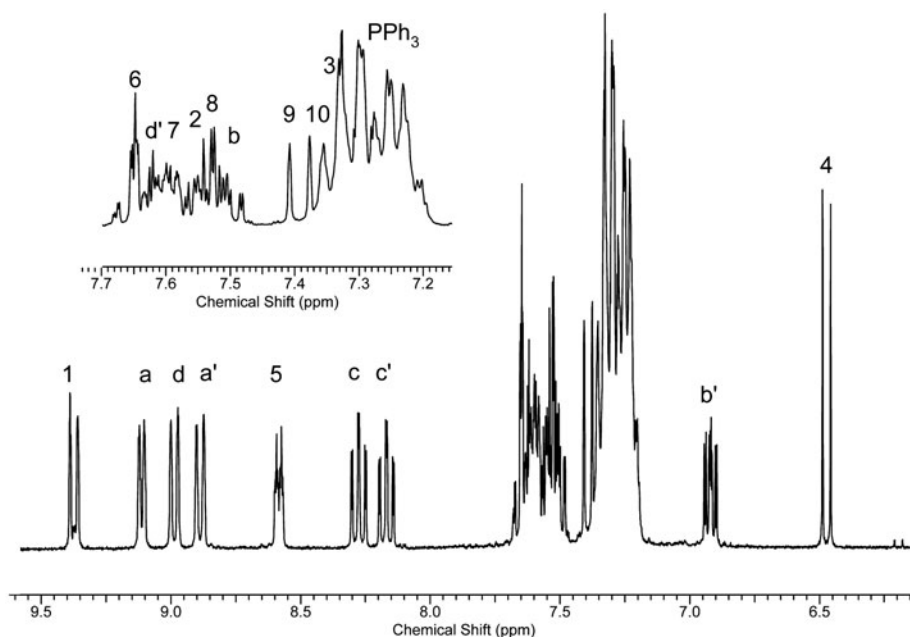
Figure 2. ^{1}H NMR spectrum of [Ru(pan)(PPh$_3$)(bpy)]PF$_6$ in d$_6$-acetone at 300 MHz.
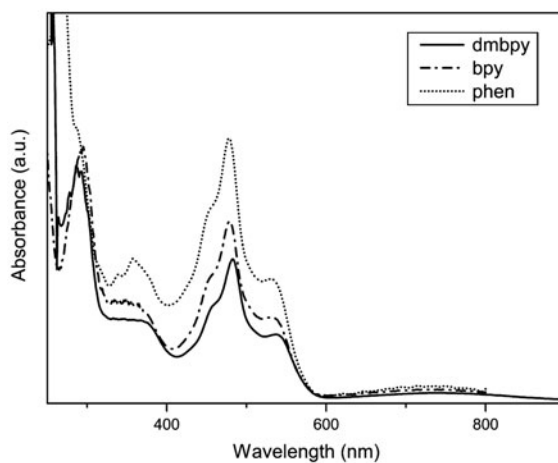
Figure 3. Experimental UV–vis spectra of (A) [Ru(pan)(PPh$_3$)(bpy)]$^+$, (B) [Ru(pan)(PPh$_3$)(dmbpy)]$^+$, and (C) [Ru(pan)(PPh$_3$)(phen)]$^+$ obtained in acetonitrile.

the spectra have intense bands due to metal-to-ligand charge-transfer transitions (MLCT) from the metal dπ orbitals to the lowest energy π* orbitals of pan [11, 12]. Since pan is the best π-acceptor ligand in these complexes, the LUMO is mainly located on the π* pan

orbitals and the LUMO energy is not significantly affected by changing the nature of the polypyridinic ligand.

According to theoretical calculations, HOMO and LUMO orbitals of $[Ru(pan)(PPh_3)(bpy)]^+$, $[Ru(pan)(PPh_3)(dmbpy)]^+$, and $[Ru(pan)(PPh_3)(phen)]^+$ are composed mainly of pan (about 80% of pan and 17% of ruthenium). The complete description of composition of the molecular orbitals of complexes can be seen in tables S4, S6, and S8. The high overlap of orbital between ruthenium and pan orbitals can be associated to non-innocent behavior [36].

Complexes with innocent ligands do not have high contribution from metal in the LUMO as observed in $[Ru(terpy)_2]^{2+}$, where the contribution of ruthenium in the LUMO is only about 8%, and in $[Ru(NH_3)_4(bpy)]^{2+}$ the contribution is 6%. However, if we compare with other complexes containing non-innocent ligands, the values are similar to ours. For example, in $[Ru(NH_3)_5NO]^{3+}$ the metal has contribution which reaches 25%, or in $[Ru(bqdi)(NH_3)_2(Cl)_2]$ this percentage is 32%.

Figueroa-Villar *et al.* have proposed that the properties of some molecules are modulated by the frontier effective-for-reaction molecular orbitals (FERMO) levels, and the characteristics of ligands in the coordination sphere can modulate these properties [37, 38]. As a consequence, the variations of energy in MLCT transitions are mainly related to the energy level of the $d\pi$ metal orbitals and π orbitals from pan.

In order to explain the bathochromic effect on the MLCT in $[Ru(pan)(bpy)Cl]$ and $[Ru(pan)(bpy)(py)]^+$ [12] (table 2), the σ-donor/π-acceptor character of L on the series $[Ru(pan)(PPh3)(L)]^+$ was analyzed. Increasing the donor character of the monodentate ligand (replacement of PPh_3 to Cl) leads to destabilization of $d\pi$ metal orbitals and induces a bathochromic effect on the MLCT transitions, reflecting a decrease in the FERMO–LUMO energy gap.

A comparison between theoretical and experimental UV–vis spectra of $[Ru(pan)(PPh_3)(bpy)]^+$ can be found in figure S2. The band at 13,661 cm^{-1} is assigned to MLCT Ru, pan $\rightarrow$ pan* (MO#179 $\rightarrow$ MO#183) and (MO#181 $\rightarrow$ MO#183), see table S3. The results from theoretical calculation show that the band at 18,869 cm^{-1} is assigned to Ru, pan $\rightarrow$ pan* (MO#178, $\rightarrow$ MO#185) and Ru, pan $\rightarrow$ bpy* (MO#182 $\rightarrow$ MO#185). Bands at 20,921 cm^{-1} and 22,124 cm^{-1} are assigned exclusively to Ru, pan $\rightarrow$ pan* (MO#179 $\rightarrow$ MO#183) and (MO#178 $\rightarrow$ MO#183), respectively. Intraligand transition $PPh_3 \rightarrow$ bpy* (MO#177 $\rightarrow$ MO#183) and MLCT Ru, pan $\rightarrow$ bpy* (MO# 178 $\rightarrow$ MO#184) are found at 27,778 cm^{-1}. All data of electronic transitions and composition of molecular orbitals are presented in tables S3 and S4. Furthermore, figure S2 exhibits plots of the frontier orbitals of $[Ru(pan)(PPh_3)(bpy)]^+$.

The profile of the electronic spectra of $[Ru(pan)(PPh_3)(dmbpy)]^+$ are similar to $Ru(pan)(PPh_3)(bpy)]^+$, as shown in figure S4. The lowest energy transition is found at 13,514 cm^{-1} and assigned to MLCT Ru $\rightarrow$ pan* (MO#190 $\rightarrow$ MO#192). Other MLCT transitions are

Table 2. Selected experimental absorption data for $[Ru(pan)(L)(bpy)]^+$ complexes.

Complex	λ_{MLCT}	ε ($10^4 \times M^{-1}$ cm^{-1})	Ref.
$[Ru(pan)(PPh_3)(bpy)]^+$	530	1.6	This work
$[Ru(pan)(py)(bpy)]^+$	595	1.1	[12]
$[Ru(pan)(Cl)(bpy)]^+$	610	1.3	[12]

located at 18,657 cm^{-1} and 20,747 cm^{-1}, and they are assigned to Ru, pan $\rightarrow$ dmbpy* (MO#188 $\rightarrow$ MO#192 and MO#190 $\rightarrow$ MO#192) and Ru $\rightarrow$pan* (MO#189 $\rightarrow$ MO#192)/ pan $\rightarrow$ pan* (MO#189 $\rightarrow$ MO#192), respectively. The band at 21,978 cm^{-1} is assigned to Ru $\rightarrow$ pan* (MO#186 $\rightarrow$ MO#191) and pan $\rightarrow$ dmbpy* (MO#190 $\rightarrow$ MO#193). The electronic transition at 27,100 cm^{-1} from MO#185 to MO#191 is attributed to PPh$_3$ $\rightarrow$ pan* and MO#186 to MO#191 to Ru, pan $\rightarrow$ pan*. All data and composition of molecular orbitals are presented in tables S5 and S6. Figure S4 shows the plots of the frontier orbitals of [Ru(pan)(PPh$_3$)(dmbpy)]$^+$.

Figure S7 presents a comparison between theoretical and experimental UV–vis spectra of [Ru(pan)(PPh$_3$)(phen)]$^+$. The transition at 13,587 cm^{-1} is assigned to Ru, pan $\rightarrow$ pan* (MO#187 $\rightarrow$ MO#189). MLTC transitions at 18,762 cm^{-1} and 20,921 cm^{-1} are assigned to Ru, pan $\rightarrow$ phen* (MO#187 $\rightarrow$ MO#190) and Ru $\rightarrow$ pan* (MO#185 $\rightarrow$ MO#189), respectively. MLCT Ru, pan $\rightarrow$ pan* are found at 22,075 cm^{-1}. Transitions from ligands are found at 27,701 cm^{-1} assigned to PPh$_3$ $\rightarrow$ phen* (MO#182 $\rightarrow$ MO#189) and pan $\rightarrow$ pan* (MO#188 $\rightarrow$ MO#192). A complete description, tables and all spectroscopic data, and composition of molecular orbitals are presented in tables S7 and S8. Furthermore, figure S6 shows the plots of the frontier orbitals of [Ru(pan)(PPh$_3$)(phen)]$^+$. There is a good correlation between experimental and theoretical data.

3.3. Electrochemistry

The complexes present one reversible oxidation process and two reversible reduction processes between −1.55 and 1.20 V, as observed in figure 4. Formal potentials for redox processes of the three complexes are presented in table 3.

According to the literature [12, 39, 40], the first oxidation process corresponds to Ru^{2+} $\rightarrow$ Ru^{3+} couple. Comparing with electrochemical data of [Ru(pan)(bpy)(L)]$^+$ [8], it was assigned the first reduction to azo of coordinated pan and the second reduction to addition of one electron in π* orbitals of coordinated polypyridine (bpy, dmbpy, or phen). In the complexes, the first reduction is centered on the azo fragment, almost not affected by nature of the polypiridyl ligands.
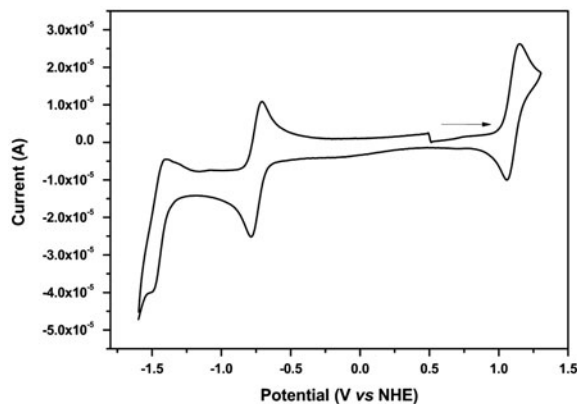

Figure 4.   Cyclic voltammogram of [Ru(pan)(PPh$_3$)bpy]$^+$ in acetonitrile. [Ru]: 1 × 10^{-3} M cm^{-3}.

Table 3.   Formal potential for the redox processes of Ru(pan)(PPh$_3$)(bpy)]$^+$, [Ru(pan)(PPh$_3$)(phen)]$^+$, and [Ru(pan)(PPh$_3$)(phen)]$^+$.

Complex	E° (V)	Assignment
Ru(pan)(PPh$_3$)(bpy)]$^+$	1.14	Ru^{II}/Ru^{III}
	−0.79	(N=N)/(N–N)$^{1-}$
	−1.49	bpy/bpy^{1-}
[Ru(pan)(PPh$_3$)(phen)]$^+$	1.13	Ru^{II}/Ru^{III}
	−0.78	(N=N)/(N–N)$^{1-}$
	−1.50	phen/phen^{1-}
[Ru(pan)(PPh$_3$)(dmbpy)]$^+$	1.10	Ru^{II}/Ru^{III}
	−0.80	(N=N)/(N–N)$^{1-}$
	−1.54	dmbpy/dmbpy^{1-}

The Ru(III/II) potential is cathodically shifted by 40 mV, due to the differences of donor character of polypyridine ligands. This decrease in the metal oxidation potential reflects the destabilization of the HOMO localized in ruthenium, caused by different donor character of the ligand which suggest an order of sigma donation, dmbpy > phen > bpy.

According to Lever, the metal oxidation potential can be calculated by summing electrochemical parameters E_L(L) of all ligands [18]. In the case of [Ru(pan)$_2$], the experimental value fits with the calculated one (0.90 V *vs.* NHE) which uses a contribution of 0.45 V for pan. This is approximately the same as that of other azopyridines and phenylazopyridine (E_L = 0.40 V), but significantly higher than that for the weaker π-acid bpy (E_L = 0.259 V) or for the π-donor oxalate (E_L = −0.17 V).

However, value of E_L for pan is not constant in the series of complexes of general formula [Ru(pan)(L)(L′)] (figure S8), as shown in table 4. For example, in [Ru(pan)(PPh$_3$)(bpy)]PF$_6$ the value of E_L for pan is +0.172 V, while for [Ru(pan)(Cl)(bpy)] [12] the value of E_L is +0.340 V.
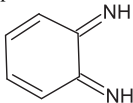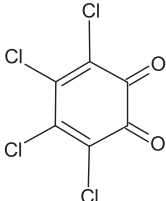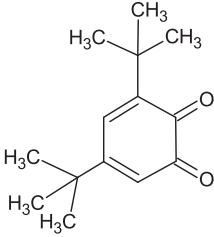
In order to understand the change of values, we need to consider the shift of ligands in the coordination sphere. In this case, PPh$_3$ is a π-acceptor ligand if compared to Cl$^-$. This change of the groups decreases the electron density in pan and interferes in the back bonding from metal to ligand (pan).

In the case of Cl$^-$, the electron density in the ruthenium is higher due to π-donation of this ligand; consequently, these interactions increase the π-acceptor character of pan. On the

Table 4.   Values of E_L for pan calculated from the Lever equation.

Complexes	E_L (pan)
[Ru(pan)(PPh$_3$)(bpy)]PF$_6$	0.172
[Ru(pan)(PPh$_3$)(phen)]PF$_6$	0.172
[Ru(pan)(PPh$_3$)(dmbpy)]NO$_3$	0.201
[Ru(pan)(pic)(bpy)]ClO$_4$	0.231
[Ru(pan)(py)(bpy)]ClO$_4$	0.243
[Ru(pan)(Cl)(bpy)]	0.34
[Ru(pan)$_2$]	0.443

Table 5. Some complexes contain non-innocent ligands and their respective values of E_L.

Ligand L	Complex	$E_L(L)$	Ref.
Bqdi	$[Ru(L)(NH_3)_2(Cl)_2]$	0.80	[37]
	$[Ru(L)(acac)_2]$	0.84	[37]
	$[Ru(L)(NH_3)_4]^{2+}$	0.36	[37]
$Cl_4C_6O_2$	$[Ru(L)(CN)(CO)_2(PPh_3)]^-$	0.65	[41]
	$[Ru(L)(CN)(CO)_2(P(OPh)_3)]^-$	−0.69	[41]
$3.5\text{-}tBu_2C_6H_2O_2$	$[Ru(terpy)(L)(CO)]^+$	−1.12	[41]
	$[Ru(terpy)(L)(DMSO)]^+$	−0.38	[41]

other hand, PPh_3 decreases the charge density in the ruthenium and the back bonding from metal to pan, which decreases π-acceptor character of pan.

Therefore, the pan fragment is susceptible to chemical influence of other ligands coordinated to ruthenium(II) [38, 41]. This feature can be observed due to the high degree of covalency of bonding metal–ligand, and the π-acceptor character is modulated in this series of complexes as demonstrated in table 5.

Spectroelectrochemistry studies were performed to corroborate the assignments proposed to electronic spectra and cyclic voltammograms. The oxidation of $[Ru(pan)(PPh_3)(L)]^+$ is reversible with greater than 90% recovery of the Ru(II) complex spectrum. For $[Ru(pan)(PPh_3)(bpy)]^+$, the visible region is dominated by strong absorbance bands centered at 530, 478, and 360 nm, and a shoulder at 452 nm which we assign by analogy to other Ru(II) azonaphthol complexes [7, 8] to Ru(II)-to-azonaphthol $d\pi$–π^* MLCT transitions. The MLCT transition of Ru(II) to bpy is predicted to be shifted to higher energy by approximately 0.7 V, which is the difference between azonaphthol and bpy reduction couples. Oxidation of the ruthenium complex leads to the decay of MLCT band in the visible region (figure 5), with new bands at 480 nm (8.0×10^3 M^{-1} cm^{-1}), 315 (11.1×10^3 M^{-1} cm^{-1}), and 303 (11.9×10^3 M^{-1} cm^{-1}) ascribed to a ligand-to-metal charge-transfer transition. The spectroelectrochemistry of $[Ru(pan)(PPh_3)(dmbpy)]^+$ and $[Ru(pan)(PPh_3)(phen)]^+$ were similar to that found for $[Ru(pan)(PPh_3)(bpy)]^+$.
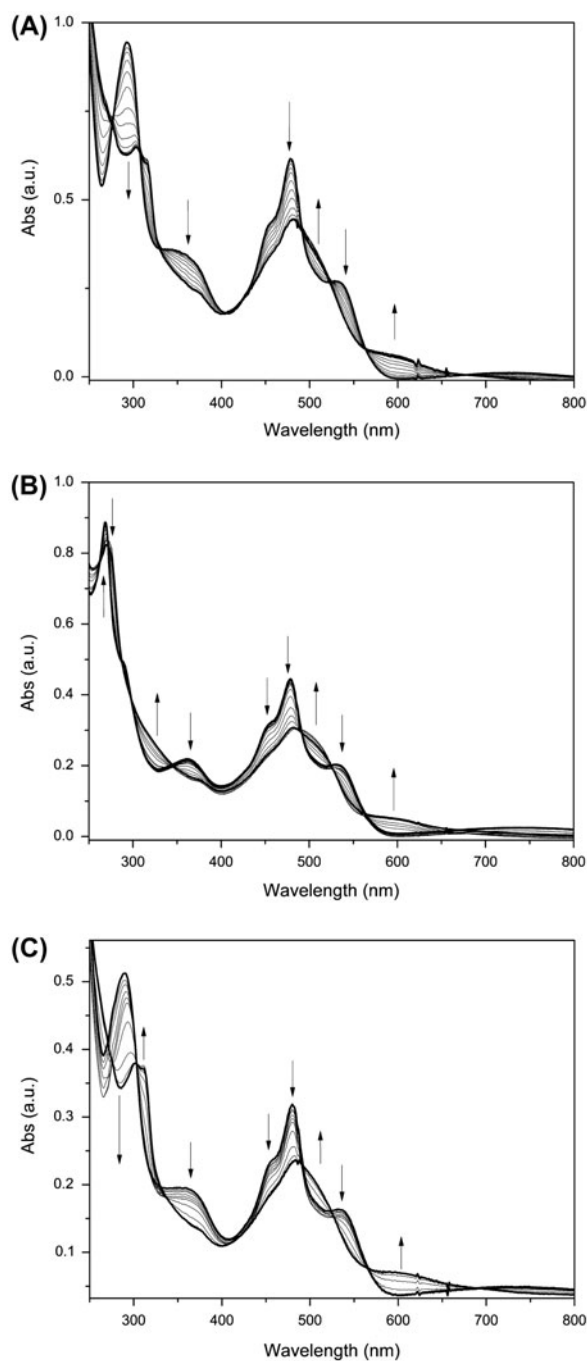
Figure 5. UV–vis spectroelectrochemistry of: (A) [Ru(pan)(PPh₃)bpy]⁺, (B) [Ru(pan)(PPh₃)(dmbpy)]⁺, and (C) [Ru(pan)(PPh₃)(phen)]⁺ in acetonitrile with potentials between 0 and 0.8 V *vs.* Ag/Ag⁺. [Ru] 5×10^{-4} M cm⁻³. The arrows indicate the modification of the spectra with the potential.

4. Conclusion

We have synthesized a series of new ruthenium(II) pan complexes bearing triphenylphosphine or polypyridine. Characterization of all the complexes was accomplished by theoretical, spectroscopic, and electrochemical studies. The non-innocent behavior of pan was observed, and it was confirmed using the electrochemical parameter $E_L(L)$ approach and supported by experimental redox data of the polypyridine ligands. Pan parameters are modulated by donor and acceptor character from other ligands in the coordination sphere, according to the non-innocent behavior of pan.

References

[1] B.J. Holliday, C.A. Mirkin. *Angew. Chem., Int. Ed.*, **40**, 2022 (2001).
[2] V. Balzani, A. Credi, F.M. Raymo, J.F. Stoddart. *Angew. Chem., Int. Ed.*, **39**, 3848 (2000).
[3] R.J. Crutchley, A.B.P. Lever. *Inorg. Chem.*, **21**, 2276 (1982).
[4] S. Srijaranai, W. Autsawaputtanakul, Y. Santaladchaiyakit, T. Khameng, A. Siriraks, R.L. Deming. *Microchem. J.*, **99**, 152 (2011).
[5] V.M. Ivanov. *J. Anal. Chem.*, **60**, 486 (2005).
[6] P. Mondal, A. Hens, S. Basak, K.K. Rajak. *Dalton Trans.*, **42**, 1536 (2013).
[7] K. Pramanik, B. Adhikari. *Polyhedron*, **29**, 1015 (2010).
[8] Z. Safari, M.B. Gholivand, L. Hosseinzadeh. *Spectrochim. Acta, Part A*, **78**, 1606 (2011).
[9] L. Szabó, K. Herman, N.E. Mircescu, A. Fălămaş, L.F. Leopold, N. Leopold, C. Buzumurgă, V. Chiş. *Spectrochim. Acta, Part A*, **93**, 266 (2012).
[10] A. Mathew, A.V.K. Kumar, P. Shyamala, A. Satyanarayana, I.M. Rao. *Indian J. Chem. Technol.*, **19**, 331 (2012).
[11] E.P. Benson, J.I. Legg. *Inorg. Chem.*, **20**, 2504 (1981).
[12] S. Basu, S. Halder, I. Pal, S. Samanta, P. Karmakar, M.G.B. Drew, S. Bhattacharya. *Polyhedron*, **27**, 2943 (2008).
[13] V.R. de Souza, A.M.D. da Costa Ferreira, H.E. Toma. *Dalton Trans.*, **3**, 458 (2003).
[14] A.C. Raimondi, V.R. de Souza, H.E. Toma, A.S. Mangrich, T. Hasegawa, F.S. Nunes. *Polyhedron*, **23**, 2069 (2004).
[15] V.R. Souza, H.R. Rechenberg, J.A. Bonacin, H.E. Toma. *Spectrochim. Acta, Part A*, **71**, 1296 (2008).
[16] A.P. da Silva, G.D. de Freitas Gauze, T.A. Matias, V.R. de Souza, T.D. de Castro Rozada, E.A. Basso. *Tetrahedron Lett.*, **52**, 5043 (2011).
[17] K. Siu, S.M. Peng, S. Bhattacharya. *Polyhedron*, **18**, 631 (1999).
[18] A.B.P. Lever. *Inorg. Chem.*, **29**, 1271 (1990).
[19] P.J. Taylor, A.A. Schilt. *Inorg. Chim. Acta*, **5**, 691 (1971).
[20] M. Haga, T. Matsumura-Inoue, K. Shimizu, G.P. Satô. *Dalton Trans.*, 371 (1989).
[21] H. Masui, A.B.P. Lever. *Inorg. Chem.*, **32**, 2199 (1993).
[22] X. Xiao, J. Sakamoto, M. Tanabe, S. Yamazaki, S. Yamabe, M.-I. Matsumura-Inoue. *J. Electroanal. Chem.*, **527**, 33 (2002).
[23] A.B.P. Lever. In *Comprehensive Coordination Chemistry, II*, A.B.P. Lever (Ed.), Vol. 2, pp. 251–268, Elsevier Science, Boston, MA (2004).
[24] A. Juris, V. Balzani, F. Barigelletti, S. Campagna, P. Belser, A. von Zelewsky. *Coord. Chem. Rev.*, **84**, 85 (1988).
[25] C.K. Jørgensen. *Coord. Chem. Rev.*, **1**, 164 (1966).
[26] M.C. Hughes, D.J. Macero. *Inorg. Chem.*, **15**, 2041 (1976).

[27] C. Rovira, X. Ribas, A. Serpe, P. Deplano. *Dalton Trans.*, **39**, 4566 (2010).
[28] M.D. Ward, J.A. McCleverty. *J. Chem. Soc., Dalton Trans.*, 275 (2002).
[29] S. Blanchard, E. Derat, M. Desage-El Murr, L. Fensterbank, M. Malacria, V. Mouriès-Mansuy. *Eur. J. Inorg. Chem.*, **2012**, 376 (2012).
[30] W. Kaim, B. Schwederski. *Coord. Chem. Rev.*, **254**, 1580 (2010).
[31] V. Lyaskovskyy, B. de Bruin. *ACS Catal.*, **2**, 270 (2012).
[32] T.A. Stephenson, G. Wilkinson. *J. Inorg. Nucl. Chem.*, **28**, 945 (1966).
[33] B. Kratochvil, E. Lorah, C. Garber. *Anal. Chem.*, **41**, 1793 (1969).
[34] M.W. Schmidt, K.K. Baldridge, J.A. Boatz, S.T. Elbert, M.S. Gordon, J.J. Jensen, S. Koseki, N. Matsunaga, K.A. Nguyen, S. Su, T.L. Windus, M. Dupuis, J.A. Montgomery. *J. Comput. Chem.*, **14**, 1347 (1993).
[35] P.J. Hay, W.R. Wadt. *J. Chem. Phys.*, **82**, 299 (1985).
[36] A.B.P. Lever. *Coord. Chem. Rev.*, **254**, 1397 (2010).
[37] R.R. da Silva, T.C. Ramalho, J.M. Santos, J.D. Figueroa-Villar. *J. Phys. Chem. A*, **110**, 1031 (2006).
[38] R.R. da Silva, J.M. Santos, T.C. Ramalho, J.D. Figueroa-Villar. *J. Braz. Chem. Soc.*, **17**, 223 (2006).
[39] R. Raveendran, S. Pal. *Polyhedron*, **24**, 57 (2005).
[40] C. GuhaRoy, S.S. Sen, S. Dutta, G. Mostafa, S. Bhattacharya. *Polyhedron*, **26**, 3876 (2007).
[41] J.L. Boyer, J. Rochford, M.K. Tsai, J.T. Muckerman, E. Fujita. *Coord. Chem. Rev.*, **254**, 309 (2010).